Application of a hybrid Eulerian-Lagrangian PIC model to focused wave interaction with WEC-type floating buoys

Qiang Chen, Haoyu Ding, and Jun Zang

Abstract—**This paper aims to provide a better understanding of the interactions between focused waves and moored wave energy converter type floating buoys. This is achieved via numerical modelling using a 3D parallel Particle-In-Cell method based model, which solves the Navier-Stokes equations for free-surface flows and incorporates a Cartesian cut cell method based coupling algorithm for fluid-structure interaction. The focused waves generated in a numerical wave tank are first validated against experimental measurements, and then used for fluid-structure interaction simulations. The effect of wave steepness of the incident focused wave and geometry of the floating buoy (including a hemispherical-bottomed cylinder and a cylinder with a moon pool) on the motion of the buoy as well as the mooring force are discussed. This paper is a participant of the CCP-WSI Blind Test Series 2 (http://www.ccp-wsi.ac.uk/).**

Keywords—**Focused wave, Particle-In-Cell method, Wave energy converters.**

I. Introduction

THIS paper is part of the CCP-WSI Blind Test Series 2 that is devised by the Collaborative Computational Project in Wave Structure Interaction (CCP-WSI) group (http://www.ccp-wsi.ac.uk/). The Workshop aims to provide a better understanding of the wide issues involved in selecting or developing numerical models for simulating the interaction of waves with offshore and coastal structures. In the previous CCP-WSI Blind Test Series 1, investigations on the focused wave interaction with a fixed FPSO (Floating Production Storage and Offloading) like structure were conducted [1]. In the current CCP-WSI Blind Test Series 2, more complex focused wave interaction with floating structures are considered. The aim of this paper is thus to test the performance of a Particle-In-Cell (PIC) method based numerical model for simulating focused wave impact on two simplified wave energy converter (WEC) type floating buoys and to provide a better understanding of the physical phenomena involved.

With the increasing demand of clean renewable energy, ocean scientists and engineers have focused on designing different type of WECs for safe and efficient access to the wave energy. Typical WEC concepts include oscillating buoys, floating ducks, enclosed chambers, snakes and flaps [2]. Amongst many other important challenges for these concepts, scientists and engineers must find ways to ensure the survivability of the WECs in rough sea conditions. This paper thus focuses on comparing the performance of two simplified oscillating buoy WECs under extreme focused wave action. The geometry of the WECs are: 1) a hemispherical-bottomed cylinder, and 2) a cylinder with a moon pool. The focused waves tested have different steepness, representing varying nonlinearities within the waves. The purpose is to assess the effect of wave steepness and float geometry on the motion of the buoy and the mooring force.

The research method used in this paper is numerical modelling through computational fluid dynamic (CFD) models. Similar works can be found in the open literature. Reference [3] simulated focused wave interaction with a hemispherical-bottomed cylinder using the mesh-based open-source tool OpenFOAM®. Their numerical results match well with physical experimental data. Reference [4] modelled similar cases using the particle-based Smoothed Particle Hydrodynamics (SPH) method. Their simulations include both non-breaking and breaking waves, and different mooring configurations that encounter either non-snatch or snatch mooring loads. Their SPH results compare well with the experiment by [5] for the non-breaking wave cases but are less accurate for breaking wave cases. Reference [6] simulated the same cases as those presented in the above papers using a hybrid particle-mesh Particle-In-Cell (PIC) method based solver. Their numerical results compare well with the experimental data by [4] and [5] for the non-breaking

This paper was submitted to wave hydrodynamic modelling section with ID number 1480. This work was supported by the UK-China joint projects ResIn (EPSRC Grant No. EP/R007519/1) and UK-CIAPP (RAE Grant No. UK-CIAPP/73), and the Open Funding of the State Key Laboratory of Coastal and Offshore Engineering at Dalian University of Technology (Grant No. LP1803). The physical data presented here was generated as part of EPSRC funded research (EP/J012866/1) and is distributed via the CCP-WSI (EP/M022382/1) through the CCP-WSI project website (http://www.ccp-wsi.ac.uk/).

Q. Chen, H. Ding and J. Zang are with Water, Environment and Infrastructure Resilience (WEIR) Group, Department of Architecture and Civil Engineering, University of Bath, Bath, UK, BA2 7AY (e-mails: chenqiang913@hotmail.com; hd484@bath.ac.uk; j.zang@bath.ac.uk).

Q. Chen is also with State Key Laboratory of Coastal and Offshore Engineering, Dalian University of Technology, Dalian, 116024, China.

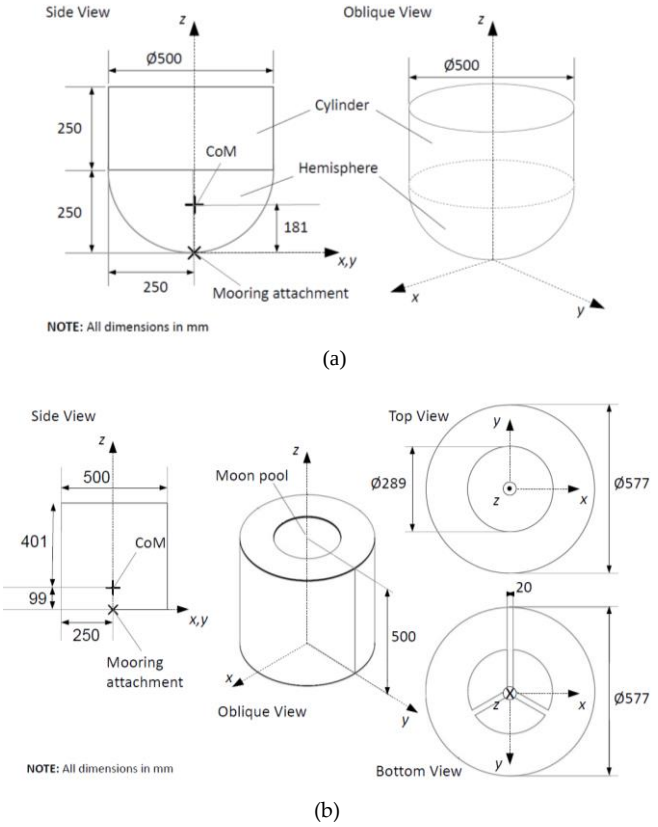

Fig. 1. Schematic showing the dimensions of the buoys: (a) Geometry 1, and (b) Geometry 2. This figure is reprinted from the CCP-WSI website (http://www.ccp-wsi.ac.uk/).

wave cases. Also, the hybrid PIC model shows a similar efficiency to the Eulerian OpenFOAM® model in terms of CPU cost. Nevertheless, in the above-mentioned numerical modelling works, the effect of wave steepness and float geometry on the motion of the buoy as well as the mooring force, as mentioned above, has not been discussed.

In this paper, the PIC model developed in [6] has been employed for the numerical simulations. The model employs both a set of Lagrangian particles and an Eulerian grid to solve the incompressible Navier-Stokes equations (NSE) for single-phase free-surface flows. The novelty of the model lies in the fact that the linear non-advection terms of the NSE are resolved on the grid, while the nonlinear advection terms are handled using the particles in a Lagrangian manner. This makes the model both efficient and flexible in terms of simulating complex physical problems such as those involving large free-surface deformations. For fluid-structure interaction, the model employs a Cartesian cut cell based two-way coupling algorithm and is able to simulate wave interaction with surface-piercing structures of arbitrary configuration and degree of freedom. More details regarding the solution procedure of the numerical model are discussed in the following section.

II. THE PIC MODEL

The PIC model solves the incompressible NSE for single-phase free-surface flows:

$$\nabla \cdot \boldsymbol{u} = \boldsymbol{0} \tag{1}$$

$$\frac{\partial \boldsymbol{u}}{\partial t} + (\boldsymbol{u} \cdot \nabla)\boldsymbol{u} = -\frac{1}{\rho}\nabla p + \upsilon \nabla^2 \boldsymbol{u} + \boldsymbol{f} \tag{2}$$

where, in 3D, $\boldsymbol{u}$ is the velocity field; t is the time; p is the pressure; $\boldsymbol{f}$ = (0.0, 0.0, -9.81 m/s²) corresponds to the body force due to gravity; ϱ and ν are the density and kinematic viscosity of the fluid, respectively.

The numerical model employs both a set of Lagrangian particles and an Eulerian grid to discretize the computational domain. The grid has a uniform size and is staggered following [7], and eight particles are initially seeded in each of the grid cells covered by the fluid phase. The particles are assigned with the mass and momentum of the fluid following [8], and are used to solve the nonlinear advection term in a Lagrangian manner and track the fluid configuration as well as the free-surface position, while the underlying grid is employed for solving the non-advection terms for computational convenience. In general, the solution procedure is divided into two major steps: an Eulerian step and a Lagrangian step. In the Eulerian step, the non-advection terms are first solved on the grid using the pressure projection method proposed in [9]. Then, in the Lagrangian step, the newly updated velocity field and a velocity change field on the grid are interpolated onto the particles to update the velocity field carried by the particles, which are then advected to solve the remaining advection term. The velocity field carried by the particles are then interpolated onto the grid at the beginning of the next time step using a SPH-like kernel interpolation that conserves the mass and momentum. For fluid-structure interaction, the numerical model employs a Cartesian cut cell method based two-way coupling algorithm, which is resolved during the Eulerian step. In addition, the numerical model is parallelized using the domain decomposition based Massage Passing Interface (MPI) approach. Note that in the current model, a laminar flow assumption is used (i.e. no turbulence model has been incorporated), as the waves investigated do not break. For full details of the current 3D parallel PIC model for wave interaction with floating bodies, the reader is referred to [6].

III. TEST CASES SETUP

In this section, the test cases of focused wave interaction with two simplified WEC-type floating buoys set out in the CCP-WSI Blind Test Series 2 website (http://www.ccp-wsi.ac.uk/) and the corresponding setup of the numerical model are introduced.

TABLE I
PROPERTIES OF THE FLOATING BUOYS AND LINEAR SPRING MOORINGS

Geometry	Mass (Kg)	Ixx, Iyy, Izz (Kg·m²)	Draft (m)	Z position of CoM	Pretension in mooring (N)	Mooring line stiffness (N/m)
1	43.674	2.219, 2.219, 1.143	0.322	-0.141	32.07	67
2	61.459	1.790, 1.790, 3.298	0.330	-0.231	31.55	67

A. Experiment setup

The physical experiments of the test cases were performed in the COAST Laboratory Ocean Basin (35 m long × 15.5 m width) at Plymouth University UK. The basin has 24 flap-type, force feedback controlled wave makers. The water depth, h, at the working area was set to 3.0 m. At the far end of the basin there is a parabolic absorbing beach for wave absorption.

The two WEC-type floating buoys, both moored with a simple linear spring mooring, have different geometries: (1) a hemispherical-bottomed cylinder (hereafter referred to as Geometry 1), and (2) a cylinder with a moon pool (hereafter referred to as Geometry 2). The complexity increases in Geometry 2 by introducing an internal body of water. Fig. 1 shows detailed structures of Geometries 1 and 2, and Table I presents the properties of the two buoys and the linear spring moorings. Note that the geometries of the structures as well as other properties such as the centre of mass and the moment of inertia may have been updated by the CCP-WSI group; while the properties and geometries presented in this paper can be considered as 'hypothetical' cases, up-to-date versions of the data can be found in the CCP-WSI Blind Test Series 2 website (http://www.ccp-wsi.ac.uk/).

Each buoy is individually subjected to the same set of incident wave cases consisting of three focused wave events with a range of steepness, kA. Table II presents the parameters of the focused waves. Each wave was created using linear superposition of 244 wave fronts with frequencies evenly spaced between 0.101563 Hz and 2 Hz and a theoretical focus location, x_0, which was calibrated to produce the desired wave shape (symmetric troughs either side of the main crest; all waves in the CCP-WSI Blind Test Series 2 are crest focused waves) at the rest position of the buoys. The amplitudes of the frequency components were derived by applying the NewWave theory to the Pierson-Moskowitz spectrum with the parameters given in Table II. It is noted that the steepness of the waves is varied parametrically by altering the peak frequency whilst maintaining the same crest height.

The measurements in the experiments include free-surface elevations, buoy motions and the mooring forces. However, because the CCP-WSI Blind Test Series 2 is a "blind" validation of numerical wave-structure interaction models, the only physical measurement data available at this time is the surface elevation data from the wave gauges in the empty tank tests (i.e. without the buoys). This data is sufficient to reproduce the incident waves in each of the cases (see Table II), which are the same as those used in the cases with the buoys in place. The remaining physical measurements will be released after completion of the CCP-WSI Blind Test Series 2 through the CCP-WSI Website (http://www.ccp-wsi.ac.uk/).

B. Numerical model setup

For the numerical simulation, the numerical wave tank (NWT) is set to 21.0 m long, 6.0 m wide and 4.0 m high in order to save on CPU cost. This relatively narrow computational domain than the physical basin is found to be acceptable as discussed in the previous work of [6], where similar cases are simulated using the PIC model. The water depth is kept at 3.0 m as in the experiment. The focused waves are generated using a piston-type wave paddle, of which the displacement is determined by the first-order wave maker theory and through applying the NewWave theory to the Pierson-Moskowitz spectrum (see details in [6]). The use of a piston-type wave paddle in the numerical model instead of a flap-type paddle as in the experiment is found to be capable of reproducing well the focused waves (see section IV). The buoy(s) is placed at the centre line of the NWT and the distance between the buoy(s) and the wave paddle is set to 6.25 m, which is much shorter than that used in the experiment. Note that in doing so, the input theoretical focus location must also be adjusted to be shorter than the experimental one in order to generate the desired waves as in the experiment (see discussions in [6]). Note that instead of using the theoretical parameters to generate the focused waves, one can also generate the desired waves based on the physical experimental data [10]. The incident waves are absorbed at the other end of the NWT, opposite to the wave paddle, using a modified relaxation approach that requires only half the relaxation zone length that a regular relaxation method would use [11]. The length of the relaxation zone is set to 11 m. It should be mentioned that the frame at the bottom of Geometry 2 (see Fig. 1), allowing the mooring attachment on the axial line, is made of three thin steel bars (0.003 m thick), which requires a very fine mesh discretization in the numerical modelling. For the current simulations, the three steel bars are simply omitted as the resources (particularly memory storage) required for using a very fine uniform

TABLE II
PARAMETERS OF THE INCIDENT FOCUSED WAVES

Test ID	A_n	f_p	kA
1BT2	0.25	0.3578	0.128778
2BT2	0.25	0.4	0.160972
3BT2	0.25	0.4382	0.193167

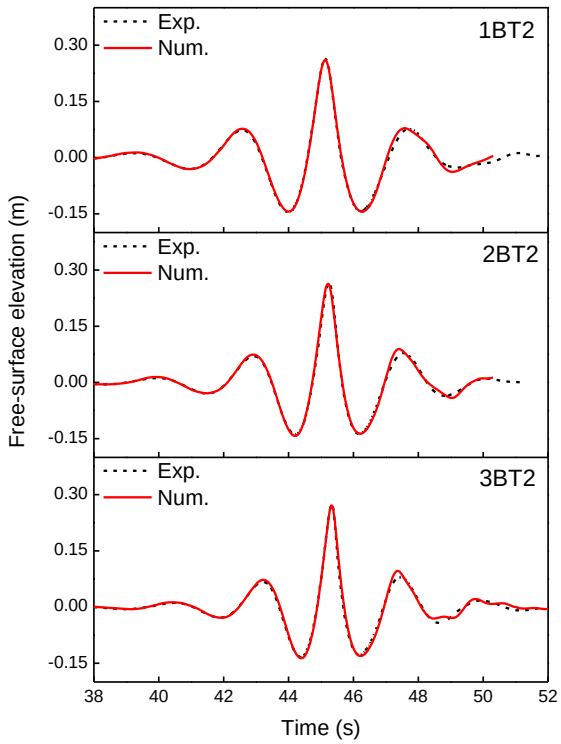

Fig. 2. Comparison between experimental and numerical results for the free-surface elevations of the incident focused waves at the rest location of the buoy(s).

mesh in the current double-grid (i.e. particle and mesh) model is unaffordable at the moment.

The grid size is set to $\Delta x = \Delta y = \Delta z = 0.025$ m according to a grid convergence study, presented in [6], on the free decay heave motion of a floating buoy with the same structure to Geometry 1. This results in approximately 32.3 million grid cells and 188.9 million particles. The Courant number is set to 0.5.

IV. Results and Discussions

In this section, the numerical results of focused wave generation are first validated against experimental measurement. Then, the numerical results of wave-structure interaction are discussed for the effect of incident wave steepness and structure geometry on the buoy motions and the mooring forces.

C. Focused wave generation

Fig. 2 shows the comparison between the numerical and experimental results for the focused wave generation without the buoy in place. The time histories of the free-surface elevations shown here are extracted at the rest location of the buoy. It is seen from Fig. 2 that the numerical model reproduces very well all of the three incident focused waves; both the peaks and the troughs of the numerical predictions of the focused wave match well with the experimental measurement. This provides a foundation for meaningful numerical results for the wave-structure interaction tests. It is also seen from Fig. 2 that as the wave steepness increases from test cases 1BT2 to 3BT2, the focused wave profile becomes more compact

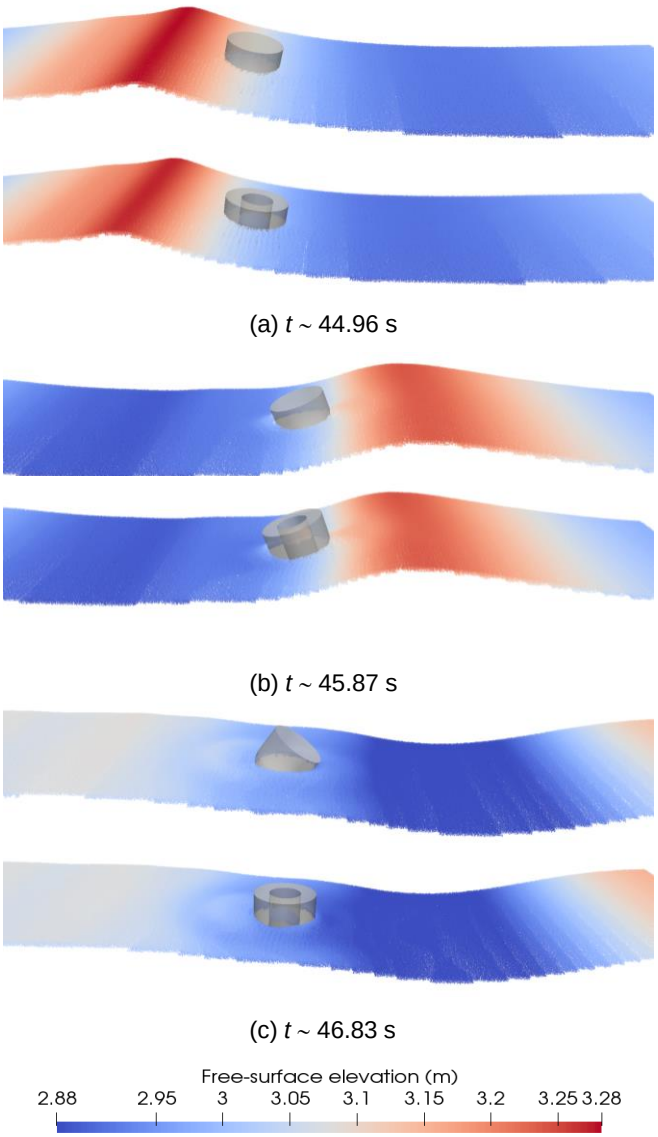

Fig. 3. Snapshots of the numerical results at different times around the impact of the main crest of the focused wave for both geometries.

(i.e. the interval of the occurring time of the wave peaks becomes shorter). We note that in general finer mesh is required to reproduce waves with higher nonlinearities. It can be confirmed from Fig. 2 that the uniform mesh size used in all of the three focused waves is acceptable.

D. Wave-structure interaction

The test cases are split into two parts: Part 1 corresponds to the focused wave interaction with Geometry 1, and Part 2 corresponds to Geometry 2 subjected to the same incident waves. As seen in Fig. 1, Geometry 2 is more complex than Geometry 1 by introducing a moon pool in the cylinder. Fig. 3 shows a comparison of the snapshots of the numerical results at various times around the impact of the main crest of the focused wave 3BT2 for both geometries. It may be seen that after the main crest has passed, the pitch motion of Geometry 1 is slightly larger than that of Geometry 2 (Fig. 3c). Also, clear evidence of the sloshing phenomenon

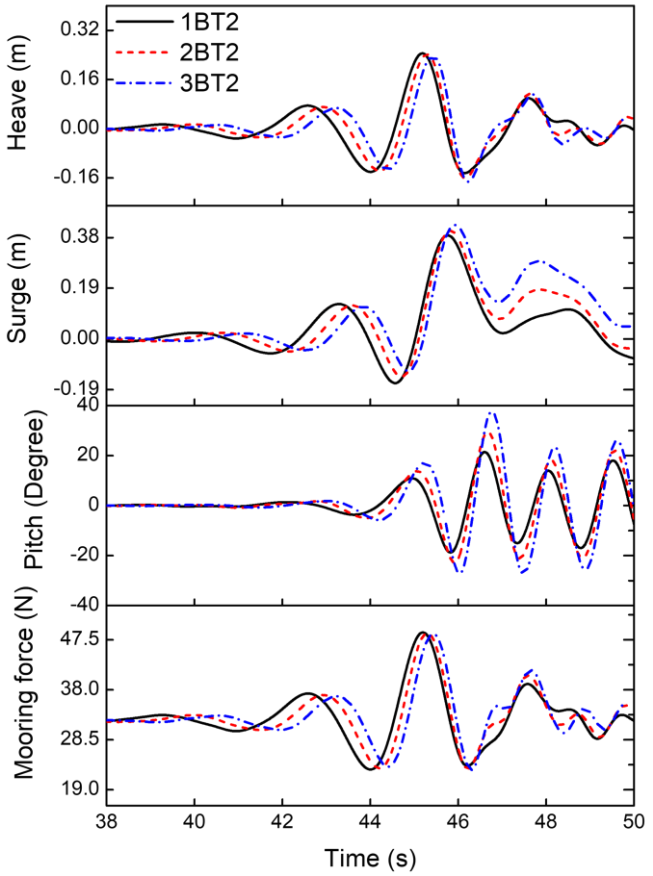

Fig. 4. Numerical results of the buoy motion (Geometry 1) and the mooring force under the focused wave action.

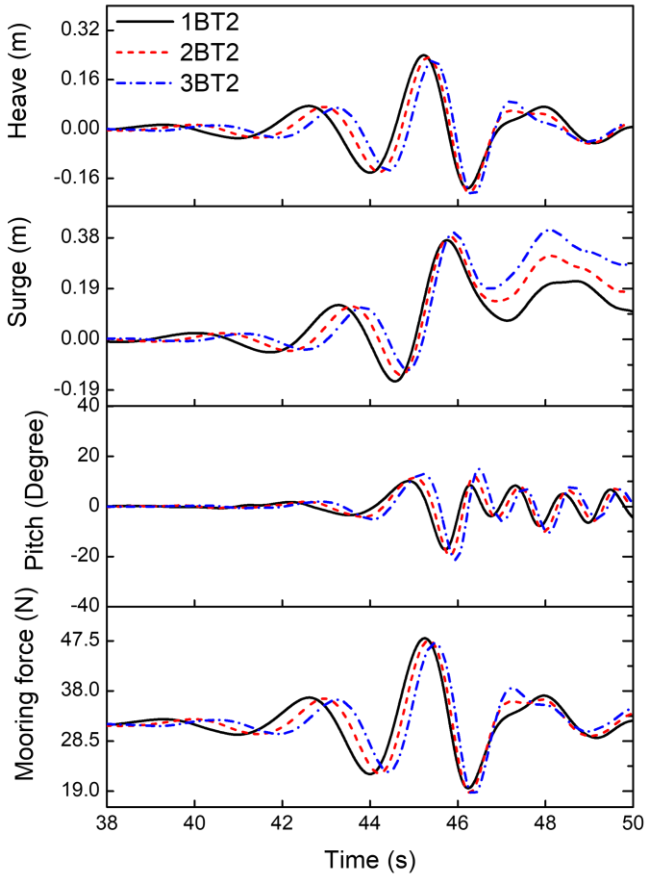

Fig. 5. Numerical results of the buoy motion (Geometry 2) and the mooring force under the focused wave action.

occurring inside the moon pool of Geometry 2 can be observed in Fig. 3b and 3c.

Fig. 4 and Fig. 5 present the numerical results of the buoy motion and the mooring force for Geometries 1 and 2 respectively, subjected to the three focused wave events. It may be seen that for both geometries the heave motions under the action of the three focused waves are quantitatively similar, meaning that the effect of wave steepness on the heave motion of the buoys is insignificant. Consequently, similar phenomenon is observed for the mooring force, which is predominantly controlled by the heave motion of the buoy. On the other hand, for both geometries, the surge and pitch motions show clear influence of the steepness of the focused wave. It is seen that in general the focused wave with larger steepness causes larger peak value of the surge displacement around t = 46 s and larger amplitude of the pitch motion during and after the main wave crest impact. For the former, this is caused by the larger wave force imposed on the buoy by the steeper waves. For the latter, it is due likely to that the peak frequency of the incident focused wave becomes closer to the natural frequencies of the geometries (~0.66 Hz for Geometry 1 and ~0.9 for Geometry 2) as it ranges from 0.36 to 0.44 for cases 1BT2 to 3BT2 (see Table II). This may also contribute to the fact that the pitch motions of Geometry 2 are in general smaller than those of Geometry 1. Another reason for the smaller pitch motion of Geometry 2 may be that this geometry tends to cause more pitch damping (including eddy making and wave radiation damping) than Geometry 1 does. It can be also observed that the third peaks of the surge displacements (around t = 48 s) increase as the wave steepness increases for both geometries. Furthermore, it is seen that the surge displacement of Geometry 2 around this time period is generally larger than those of Geometry 1. This may be because that the mooring forces for Geometry 2 around the trough after the main wave crest (t ~ 46.5 s, see Fig. 3) are smaller than those for Geometry 1, which is caused by the larger negative heave displacements around this time instant. In addition to that, Geometry 2 is much heavier. These make Geometry 2 more difficult to be pulled back after the main wave crest impact.

V. CONCLUSION

As part of the CCP-WSI Blind Test Series 2 organized by the CCP-WIS group, this paper presents a numerical study of focused wave impact on two simplified WEC-type floating buoys using the 3D parallel PIC model developed in [6]. The numerical results generally show that the wave steepness of the focused wave has a minor effect on the heave motion of the buoys as well as the mooring forces. On the other hand, larger pitch motions are observed for both geometries as the peak frequency of the incident focused wave approaches the pitch natural frequencies of the geometries. Also, larger wave

steepness leads to larger surge displacement for both geometries. The geometry of the buoy also has an effect on the surge displacement; the heavier Geometry 2 tends to drift further away from the rest location than Geometry 1. The numerical results show, however, no conclusive evidences of the effect of the internal water body of Geometry 2, which needs further investigations.

ACKNOWLEDGEMENT

This work made use of the Balena High Performance Computing (HPC) Service at the University of Bath.

REFERENCES

[1] E. Ransley, S. Yan, S. Brown, T. Mai, D. Graham, *et al.*, "Numerical simulation of focused wave interactions with a fixed FPSO-like structure - a comparative study: Results from the CCP-WSI Blind Test Series 1," *International Journal of Offshore and Polar Engineering (manuscript in press),* 2018.

[2] A. G. L. Borthwick, "Marine Renewable Energy Seascape," *Engineering,* vol. 2, pp. 69-78, Mar 2016.

[3] E. J. Ransley, D. Greaves, A. Raby, D. Simmonds, and M. Hann, "Survivability of wave energy converters using CFD," *Renewable Energy,* vol. 109, pp. 235-247, Aug 2017.

[4] S. J. Lind, P. K. Stansby, and B. D. Rogers, "Fixed and moored bodies in steep and breaking waves using SPH with the Froude–Krylov approximation," *Journal of Ocean Engineering and Marine Energy,* vol. 2, pp. 331-354, August 01 2016.

[5] M. Hann, D. Greaves, and A. Raby, "Snatch loading of a single taut moored floating wave energy converter due to focussed wave groups," *Ocean Engineering,* vol. 96, pp. 258-271, Mar 1 2015.

[6] Q. Chen, J. Zang, D. Ning, C. Blenkinsopp, and J. Gao, "A 3D parallel Particle-In-Cell solver for extreme wave interaction with floating bodies," *Ocean Engineering,* vol. 179, pp. 1-12, May 1 2019.

[7] F. H. Harlow and J. E. Welch, "Numerical Calculation of Time-Dependent Viscous Incompressible Flow of Fluid with Free Surface," *Physics of Fluids,* vol. 8, pp. 2182-2189, 1965.

[8] J. U. Brackbill and H. M. Ruppel, "FLIP: A Method for Adaptively Zoned, Particle-in-Cell Calculations of Fluid Flows in Two Dimensions," *Journal of Computational Physics,* vol. 65, pp. 314-343, Aug 1986.

[9] A. J. Chorin, "Numerical solution of the Navier-Stokes equations," *Mathematics of computation,* vol. 22, pp. 745-762, 1968.

[10] J. Zang, R. Gibson, P. H. Taylor, R. E. Taylor, and C. Swan, "Second order wave diffraction around a fixed ship-shaped body in unidirectional steep waves," *Journal of Offshore Mechanics and Arctic Engineering-Transactions of the Asme,* vol. 128, pp. 89-99, May 2006.

[11] Q. Chen, D. M. Kelly, and J. Zang, "A modification to the relaxation approach for efficient wave absorption in numerical wave tanks," *Ocean Engineering,* 2019 (Under Review).